Taylor & Francis
Taylor & Francis Group

Automatika

Journal for Control, Measurement, Electronics, Computing and Communications

ISSN: 0005-1144 (Print) 1848-3380 (Online) Journal homepage: http://www.tandfonline.com/loi/taut20

Assessment of the human exposure to transient and time-harmonic fields using the enhanced transmission line theory approach

A. Laissaoui, B. Nekhoul, S. Mezoued & D. Poljak

To cite this article: A. Laissaoui, B. Nekhoul, S. Mezoued & D. Poljak (2017) Assessment of the human exposure to transient and time-harmonic fields using the enhanced transmission line theory approach, Automatika, 58:4, 355-362, DOI: 10.1080/00051144.2018.1435341

To link to this article: https://doi.org/10.1080/00051144.2018.1435341

Published online: 22 Mar 2018.

AUTOMATIKA, 2017
VOL. 58, NO. 4, 355–362
https://doi.org/10.1080/00051144.2018.1435341

Taylor & Francis
Taylor & Francis Group

REGULAR PAPER

OPEN ACCESS Check for updates

Assessment of the human exposure to transient and time-harmonic fields using the enhanced transmission line theory approach

A. Laissaoui[a,b], B. Nekhoul[b], S. Mezoued[a] and D. Poljak[c]

[a]Faculty of Electronics and Informatics, USTHB University, Alger, Algeria; [b]Faculty of Science and Technology, University of Jijel, Jijel, Algeria; [c]Faculty of Electrical Engineering, Mechanical Engineering and Naval Architecture, University of Split, Split, Croatia

ABSTRACT

The paper deals with the assessment of human exposure to the transient electromagnetic fields and high-frequency (HF) radiation. The formulation of the problem is based on a simplified cylindrical representation of the human body. The analysis is based on the enhanced transmission line (TL) theory. For this purpose, in order to quantify the induced current inside the human body, we solve linear system equations, where the electromagnetic field excitation is represented by two equivalent current and voltage generators. Once the axial current is determined, it is possible to calculate the specific absorption rate (SAR). Some illustrative computational examples are presented in the paper.

ARTICLE HISTORY
Received 18 April 2017
Accepted 23 January 2018

KEYWORDS
Human exposure; transient field; transmission line approach; specific absorption rate; current density

1. Introduction

In the last 60 years, electricity requirements in the world have multiplied by twelve. Electricity has become an indispensable partner in our daily lives, our technological and economic development. Despite all the benefits associated with its use, as humans are constantly immersed in electromagnetic fields generated by different sources (power lines, mobile phones and broadcast antennas), there has been an increasing concern regarding the potential adverse health effects due to exposure to these fields. Consequently, there is a need to define safe exposure limits for both professional and general population.

To achieve this aim, it is especially crucial to provide researchers in Life Sciences objective evidence to quantify the electromagnetic phenomena occurring inside the human body and causing potential biological effects.

In addition to accurate, but at the same time computationally demanding, three-dimensional anatomical body models [1,2], some simplified models for rapid engineering estimation of the phenomena are also available, e.g. cylindrical body representation [3], involving numerical solution of Pocklington integro-differential equation using the Galerkin–Bubnov boundary element method (GB-BEM) [3,4].

The present study extends the work reported in [5], by representing the body in terms of wire-junction models to account for the influence of arms. The formulation is based on the transmission line (TL) equations in the frequency domain [6] and valid for a range frequency of 50 Hz to 110 MHz.

This paper is organized as follows: first, the axial current distribution induced along the body exposed to transient electromagnetic fields, taking into account the influence of the arms, is evaluated. Furthermore, a rapid estimation of specific absorption rate (SAR) in human body exposed to a high-frequency (HF) radiation is carried out.

2. Body models

Two representations of the human body are considered in this work: cylindrical body model and wire-junction model of the body. The human body assumed to be homogeneous is represented by a vertical cylinder of height L and radius a perpendicular to a ground plane with arms in contact with the body as shown in Figure 1, where the electrical properties of the human body such as conductivity σ and relative permittivity ε_r are assumed the same value for all organs of the body (homogeneous body).

Furthermore, the body in a direct contact with the ground is considered, as shown in Figure 2. The arms are represented by a set of wires connected to the thick cylinder. The dimensions are given in Table 1.

The per unit length parameters of the horizontal segments are calculated using the formalism of Ametani et al. [7]. For vertical segments, we use the formalism of Rogers et al. [8].

3. Transmission line formulation

The TL theory allows the study of propagation phenomena along a slender support. The voltage and the

CONTACT D. Poljak dpoljak@fesb.hr

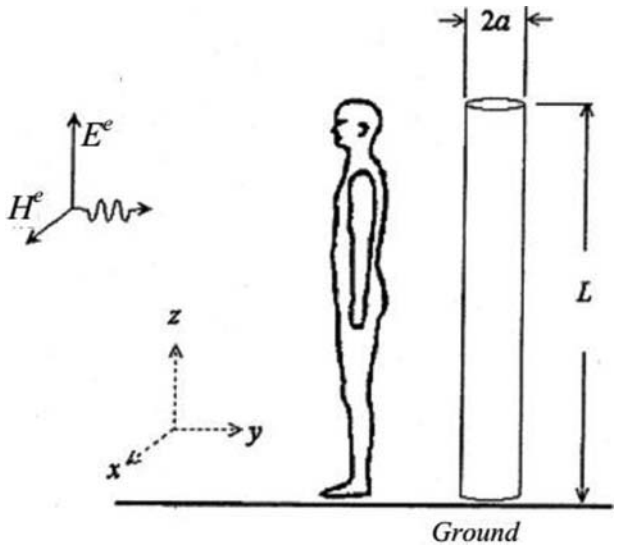

Figure 1. The cylindrical model of the human body exposed to an external electromagnetic field.

current distribution along the TL are governed by Telegraph equations.

The set of equations accounting for the coupling between a TL (n conductors) and an external electromagnetic field is given as follows [9]:

$$\frac{d[U(z,\omega)]}{dz} + [Z]\,[I(z,\omega)] = [U_F(z,\omega)], \qquad (1)$$

$$\frac{d[I(z,\omega)]}{dz} + [Y]\,[U(z,\omega)] = [I_F(z,\omega)], \qquad (2)$$

where $[U(z,\omega)]$ and $[I(z,\omega)]$ are n-order complex vectors containing total voltage and current along the TL; $[Z]$ and $[Y]$ square matrices of order n, impedance and admittance per unit length complex. The expressions for the linear longitudinal impedance $[Z]$ and admittance per unit length transverse $[Y]$ used in this study are documented in detail in [9,10]. $[U_F(z,\omega)]$ and $[I_F(z,\omega)]$ are complex vectors due to any external electromagnetic field, where

$$[U_F(z,\omega)] = -\frac{\partial}{\partial z}\left[E_T^e(z,\omega)\right] + \left[E_L^e(z,\omega)\right], \qquad (3)$$

$$[I_F(z,\omega)] = -[Y]\left[E_T^e(z,\omega)\right], \qquad (4)$$

$[E_T^e(z,\omega)]$: sources due to incident transverse electric field;

$[E_L^e(z,\omega)]$: sources due to incident longitudinal electric field.

In our work, only the vertical incident electric field (longitudinal) to the human body is of interest. The vertical field E_z^e is the main cause of the exposition; the prevailing direction of induced currents and voltages is also vertical (axial).

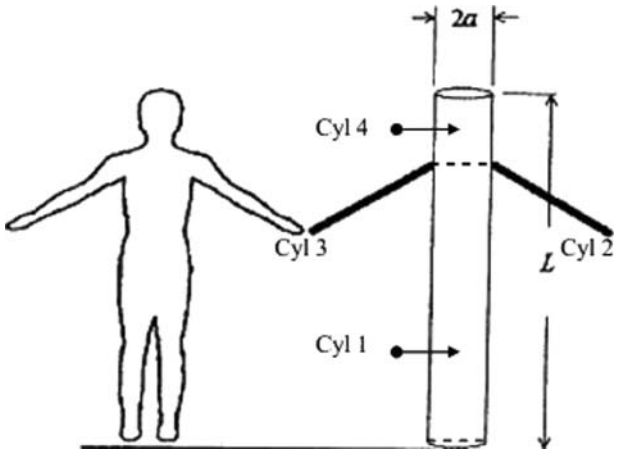

Figure 2. Model of the human body with arms outstretched.

Table 1. Geometric parameters.

	Length L_i (m)	Radius a_i (m)
Cylinder1 (body)	1.5	0.14
Cylinder 2/Cylinder3 (arms)	0.5	0.04
Cylinder 4 (head)	0.3	0.14

3.1. Solution of the transmission line equations in the frequency domain

The telegraph equations (1) and (2) can be written in state variable forms as a coupled first-order, ordinary differential equations in matrix form as

$$\underbrace{\frac{d}{dz}\begin{bmatrix}[U(z)]\\ [I(z)]\end{bmatrix}}_{X(z)} = \underbrace{\begin{bmatrix}[0] & -[Z]\\ -[Y] & [0]\end{bmatrix}}_{A}\underbrace{\begin{bmatrix}[U(z)]\\ [I(z)]\end{bmatrix}}_{X(z)} + \begin{bmatrix}[U_F(z)]\\ [I_F(z)]\end{bmatrix}. \qquad (5)$$

Note that writing Equations (1) and (2) in the matrix form provides the solution of system (5) to be obtained directly by analogy with the formalism of state variables, whose demonstration is carried out in the work of Paul [6–10]. Thus, the solution of (5) is given by

$$X(z) = \varphi(z - z_0)\,X(z_0) + \int_{z_0}^{z} [\varphi(z-\tau)]\begin{bmatrix}[U_F(\tau)]\\ [I_F(\tau)]\end{bmatrix} d\tau \qquad (6)$$

with $X(z) = \begin{bmatrix}U(z)\\ I(z)\end{bmatrix}$, matrix of voltages and currents at any point z of the TL (the body in our case).

The chain parameter matrix $[\varphi(z)]$ is defined as

$$[\varphi(z)] = e^{A.z} = \begin{bmatrix}[\varphi_{11}(z)] & [\varphi_{12}(z)]\\ [\varphi_{21}(z)] & [\varphi_{22}(z)]\end{bmatrix}. \qquad (7)$$

Note that (6) provides the values of currents and voltages at an arbitrary point z of the line according to their value at the origin z_0.

In the case studied in this work, values of voltages and currents at the extremities of the line (human body in our case) are of interest. Thus, (6) corresponding to a line that starts with $z_0 = 0$ and applied to the end $z_L = l$ becomes

$$X(l) = \varphi(l)\,.X(0) + \int_0^l [\varphi(l-\tau)] \begin{bmatrix} [U_F(\tau)] \\ [I_F(\tau)] \end{bmatrix} d\tau. \quad (8)$$

The $n \times n$ submatrices of the chain parameter matrix are given by [6]

$$[\varphi_{11}(l)] = \frac{1}{2}[Y]^{-1}[T]\left(e^{[\gamma(l)]} + e^{-[\gamma(l)]}\right)[T]^{-1}[Y], \quad (9.a)$$

$$[\varphi_{12}(l)] = -\frac{1}{2}[Y]^{-1}[T][\gamma]\left(e^{[\gamma(l)]} - e^{-[\gamma(l)]}\right)[T]^{-1}, \quad (9.b)$$

$$[\varphi_{21}(l)] = -\frac{1}{2}[T]\left(e^{[\gamma(l)]} - e^{-[\gamma(l)]}\right)[\gamma]^{-1}[T]^{-1}[Y], \quad (9.c)$$

$$[\varphi_{22}(l)] = \frac{1}{2}[T]\left(e^{[\gamma(l)]} + e^{-[\gamma(l)]}\right)[T]^{-1}, \quad (9.d)$$

where $[T]$ is a matrix of size $n \times n$; $[\gamma]$ represents the diagonal matrix of propagation constants squared with $[\gamma^2] = [T]^{-1}[Y][Z][T]$.

The development of Equation (8) allows to show the terms $U(0)$, $I(0)$, $U(l)$ and $I(l)$:

$$\begin{bmatrix} [U(l)] \\ [I(l)] \end{bmatrix} = \begin{bmatrix} [\varphi_{11}(l)] & [\varphi_{12}(l)] \\ [\varphi_{21}(l)] & [\varphi_{22}(l)] \end{bmatrix} \begin{bmatrix} [U(0)] \\ [I(0)] \end{bmatrix} + \begin{bmatrix} [U_{FT}(l)] \\ [I_{FT}(l)] \end{bmatrix} \quad (10)$$

which can be written as follows:

$$[I_{2n}] \cdot \begin{bmatrix} [U(l)] \\ [I(l)] \end{bmatrix} - \begin{bmatrix} [\varphi_{11}(l)] & [\varphi_{12}(l)] \\ [\varphi_{21}(l)] & [\varphi_{22}(l)] \end{bmatrix} \begin{bmatrix} [U(0)] \\ [I(0)] \end{bmatrix} = \begin{bmatrix} [U_{FT}(l)] \\ [I_{FT}(l)] \end{bmatrix} \quad (11)$$

where $[I_{2n}]$ is the identity matrix of order $2n$ (n: number of conductors by line).

And the total forcing functions are given in [6]:

$$[U_{FT}(l)] = \int_0^l ([\varphi_{11}(l-\tau)][U_F(\tau)] + [\varphi_{12}(l-\tau)][I_F(\tau)])d\tau, \quad (12)$$

$$[I_{FT}(l)] = \int_0^l ([\varphi_{21}(l-\tau)][U_F(\tau)] + [\varphi_{22}(l-\tau)][I_F(\tau)])d\tau. \quad (13)$$

For the case where the body is exposed to an external electromagnetic field: $[U_F(\tau)] = [E_z^e]$ and $[I_F(\tau)] = [0]$, Equations (12) and (13) become

$$[U_{FT}(l)] = \int_0^l \left([\varphi_{11}(l-\tau)]\,[E_z^e(\tau)]\right)d\tau, \quad (14)$$

$$[I_{FT}(l)] = \int_0^l \left([\varphi_{21}(l-\tau)]\,[E_z^e(\tau)]\right)d\tau. \quad (15)$$

3.2. Incorporation of boundary conditions

Obtaining the general solution of the TL coupling equations in terms of the chain parameter matrix and the external-field excitation, one then incorporates the boundary conditions to obtained corresponding voltages and currents for a given problem of interest. At both ends of the line, we have the following relationships:

$$[U(0)] = -[Z_0]\,[I(0)], \quad (16)$$

$$[U(l)] = [Z_L]\,[I(l)], \quad (17)$$

where $[Z_0]$ and $[Z_L]$ are the impedance matrices termination of the line.

In the present work, two specific ends representing the feet and head are considered. The contact of the human body with the ground can be taken into account via a capacitance C [3]:

$$Z_0 = \frac{1}{j\omega C},\ C = \frac{A\varepsilon_0\varepsilon_r}{d} \text{ and } A = \pi a^2, \quad (18)$$

where C is the capacitance between the sole of the foot and its image in the ground, ε_0 is the permittivity of free space, ε_r is the relative permittivity of the material constituting the sole of the shoe, A is the contact surface and d is the distance between the sole of the shoe and its image in the ground.

The other end of the equivalent cylinder is connected by an impedance of great value, i.e. $Z_L = \infty$. Namely, cylinders 2, 3 and 4 in the case of the human body with the arms outstretched.

3.3. Extension to multiple wire model

The principle of the proposed concept is to transform the propagation equation (10) for all the conductors representing the body and the electric relations in the all nodes to a matrix: equation system:

$$[A]\,[X] = [B]. \quad (19)$$

The matrix $[A]$ is the topological matrix of a radial network. Note that the human is considered in our work as a radial network of TL.

$[X]$ is the vector contains the unknown currents and voltages at each node;
$[B]$ is the vector includes the external field effects.

Hence, one should transform the propagation relations (11) for all the lines representing the body and the relations in the all nodes (between different organs) to matrix equation (19).

The matrix $[A]$ is composed of two submatrices:

$$[A] = \begin{bmatrix} [A_1] \\ [A_2] \end{bmatrix}.$$

The submatrix $[A_1]$ takes into account the propagation in all line segments which form the human body (trunk and arms) and constructed from Equation (11).

The submatrix $[A_2]$ takes into account the electrical relations (current and voltage) on all nodes of the human body topology [6]. Applying the Kirchhoff law in each mth node, the following equation is obtained [6]:

$$\sum_{i=1}^{N} \left(\left[Y_i^m\right] \left[U_i^m\right] + \left[Z_i^m\right] \left[I_i^m\right] \right) = [0], \qquad (20)$$

where $\left[Z_i^m\right]$ and $\left[Y_i^m\right]$ are, respectively, the impedances and admittances matrices resulting from the application of Kirchhoff's laws in the mth node. They contain the numerical values 0, 1, −1, impedances and admittances values according to the human body topology.

Finally, solving the matrix system (19) yields the currents and voltages at all nodes of the human body topology.

4. Computational examples

The computational examples are related to the body exposure to transient and to HF radiation, respectively.

4.1. Cylindrical body exposed to transient electromagnetic pulse

The human body is represented by a cylinder of length L = 1.75 m and radius a = 0.14 m. The base and the top of the cylinder are terminated by impedances Z_L and Z_0, as depicted in Figure 3.

In all calculations, the body is assumed to be well grounded, thus neglecting the capacitance between the soles of the feet and their image in the earth (Z_0 = 0 Ω), while the average value of the conductivity is chosen to be $\sigma = 0.5$ S/m (conductivity at 60 Hz).

The body is exposed to transient incident electric field in the form of double-exponential electromagnetic pulse (EMP) [11]:

$$E^e = E_0\left(e^{-\alpha t} - e^{-\beta t}\right), \qquad (21)$$

where E_0 = 1.05 V/m, $\alpha = 4 \times 10^6\ \mathrm{s}^{-1}$ and $\beta = 4.76 \times 10^8\ \mathrm{s}^{-1}$;

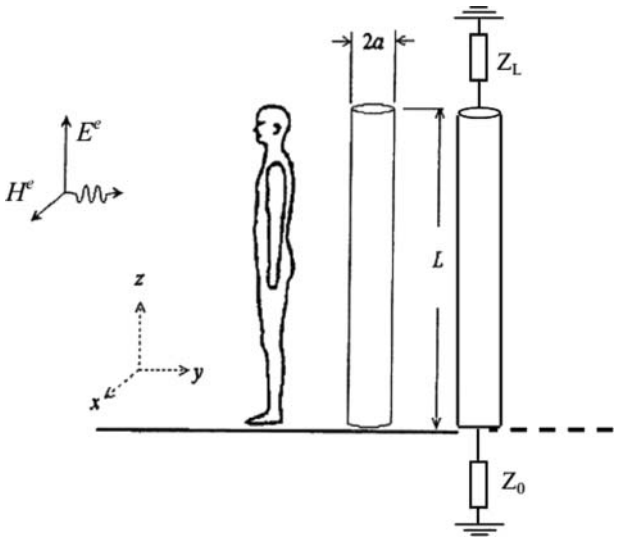

Figure 3. (a) Cylindrical model of the human body exposed to vertical electric field, (b) impedance Z_L and Z_0 on both ends of the cylinder.

The incident field is vertically polarized to ensure maximum coupling with the body. It should be noted that the exposure duration is 100 ns.

Figure 4(a,b) represents, respectively, the transient-induced current in the feet computed via the proposed TL approach compared to the direct time domain antenna theory approach based on the space-time Hallen integral equation solved via Galerkin–Bubnov indirect boundary element method (GB-IBEM) [11].

The results obtained via different approaches are found to be in a rather satisfactory agreement. In addition to plausible agreement in both the waveform and amplitude, the advantage of TL modelling is its mathematical simplicity and low computational cost. Figure 5 shows the spatial-temporal distribution of the induced current in the feet.

4.2. Human body with the arms outstretched

This subsection deals with the study of the human body with arms outstretched exposed to the bi-exponential pulse. Figures 6 and 7 represent the variation of transient current induced in the feet, the free end of the left and right arms, and the head due to exposure to the bi-exponential pulse. In this case, the current flows through the path of the least resistance [12].

Figure 6 shows a slight increase in the current induced in the feet compared to the result (Figure 4 (a)) obtained for the same excitation scenario but for the human body represented by a simple cylinder with arms in close contact with the body.

Furthermore, the human body is exposed to transient electric field in the form of Gaussian pulse [11]:

$$E_z^e(t) = E_0 e^{-g^2(t-t_0)}, \qquad (22)$$

where E_0 = 1 V/m, $g = 2 \times 10^9\ \mathrm{s}^{-1}$ and t_0 = 2 ns.

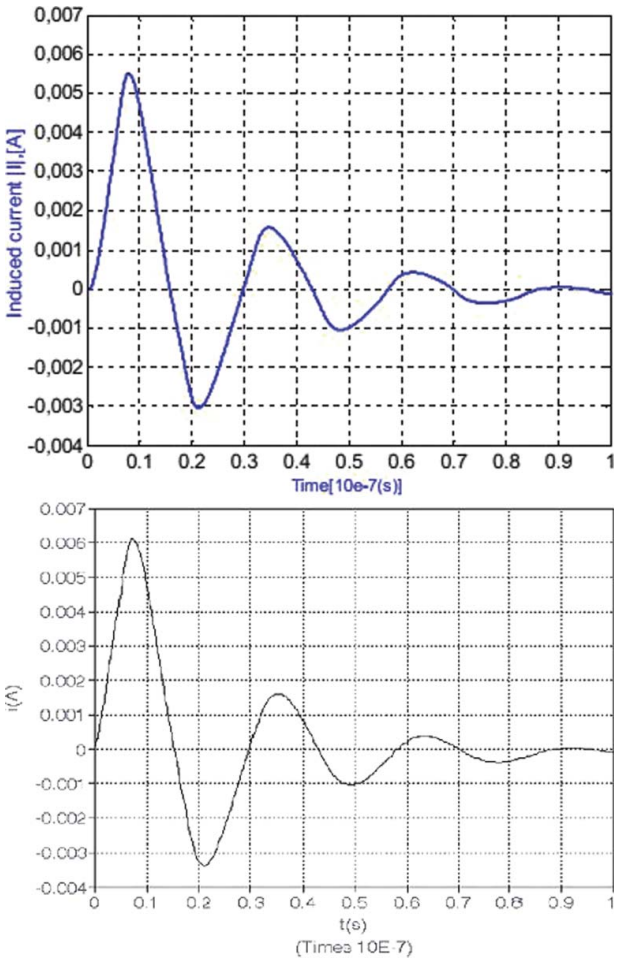

Figure 4. (a) Transient current induced in the feet due to the double exponential pulse exposure. (b) Transient current induced in the feet due to the double exponential pulse exposure (antenna model) [11].

Figure 8 shows the transient current induced in the feet due to the Gaussian pulse exposure. The transient current induced in the free end of the left/right arms and head is presented in Figure 9.

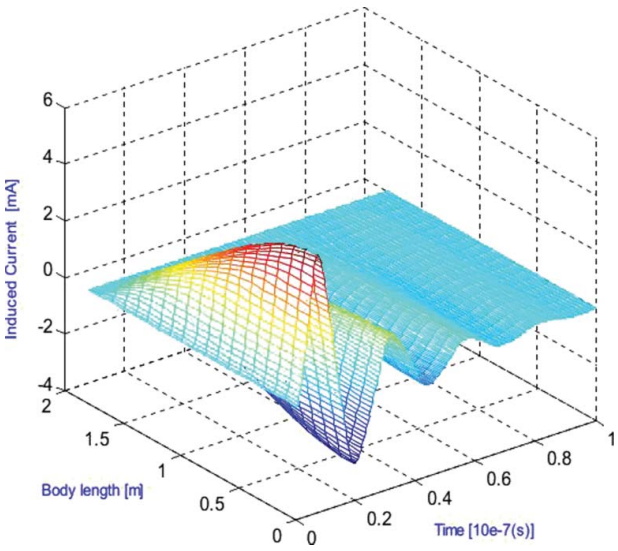

Figure 5. Spatial and temporal distribution of the induced current in the human body.

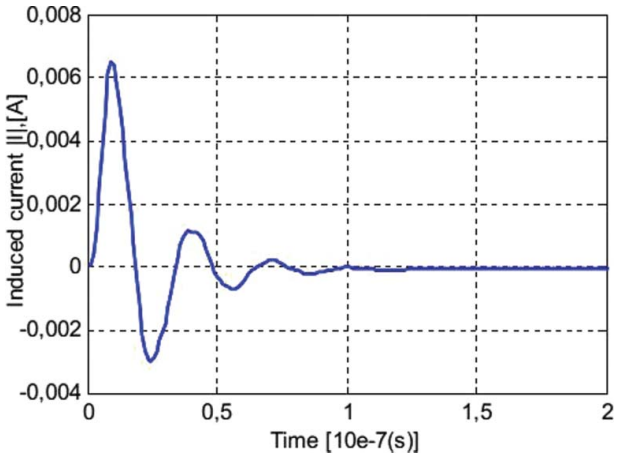

Figure 6. Transient current induced in the feet due to due to the bi-exponential pulse exposure.

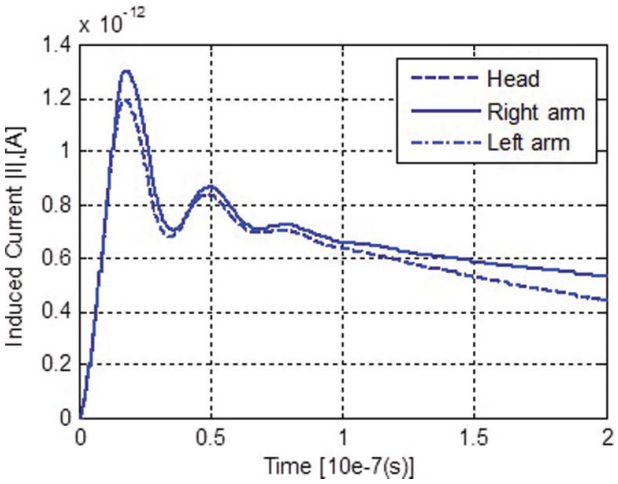

Figure 7. Transient current induced in the right arm, left arm and head due to the bi-exponential pulse exposure.

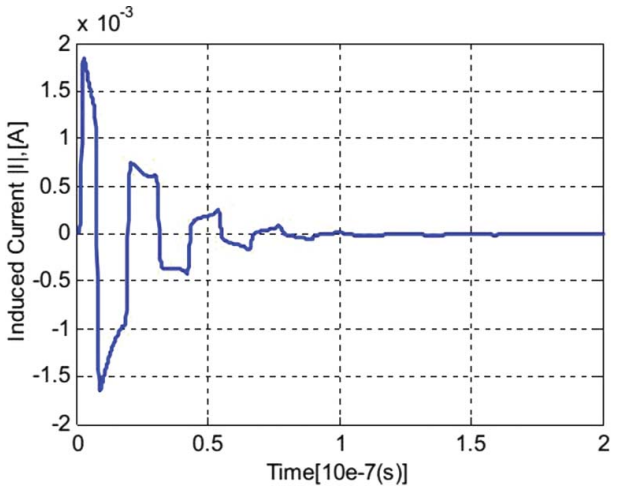

Figure 8. Transient current induced in the feet due to the Gaussian pulse exposure.

4.3. *Human exposure to high-frequency (HF) radiation*

The thermal effect of the human exposure to HF radiation is quantified in terms of the SAR.

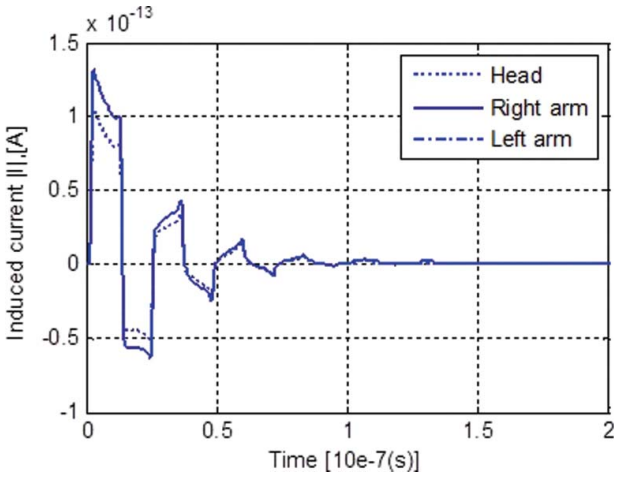

Figure 9. Transient current induced in the right arm, left arm and head due to the Gaussian pulse exposure.

The SAR (W/kg) at any point in the human head is defined as [13]

$$\mathrm{SAR} = \frac{\sigma \,|\, E \,|\,^2}{2 \cdot \rho}, \tag{23}$$

where σ and ρ are electric conductivity and density of the biological tissue, respectively, $|E|$ is the maximal value of the electric field induced in the human body.

The current density induced in the body can be expressed in terms of the axial current I_z as follows [13]:

$$J_z(r,z) = \frac{I_z(z)}{a^2\pi}\left(\frac{ka}{2}\right)\frac{J_0(j^{-1/2}k\cdot r)}{J_1(j^{-1/2}k\cdot a)}, \tag{24}$$

where J_0 and J_1 are the Bessel functions, k is the free space phase constant.

The induced electrical field is given by [13]:

$$E_z(z) = \frac{J_z(r,\ z)}{\sigma + j\omega\varepsilon}. \tag{25}$$

The basic restrictions (SAR) of the ICNIRP guidelines for frequencies between 100 KHz and 100 MHz [14], given in Table 2, are established to account for uncertainties related to individual sensitivities, environmental conditions, and for the fact that the age and health status of members of the public varies.

In this case, a man with arms in contact of the sides standing on the earth, exposed to HF radiation where the value of the uniform electrical field is found to be 1 V/m at a frequency of 30 MHz, is represented by a

Table 2. ICNIRP basic restrictions.

Frequency range 100 KHz–100 MHz	Whole body averaged SAR (W/kg)	Localized SAR (head and trunk) (W/kg)	Localized SAR (limbs) (W/kg)
General population	0.4	10	20
Occupational	0.08	2	4

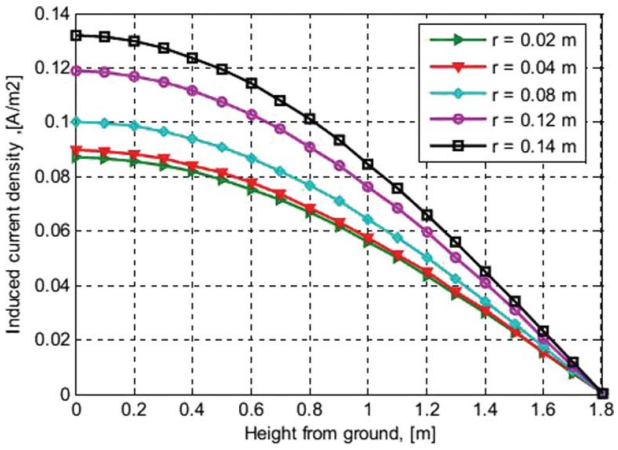

Figure 10. Current density inside the human body E_z = 1 V/m, f = 30 MHz.

cylinder of the entire length L and radius a. The average value of the conductivity and permittivity of the human body, respectively, is assumed to be $\sigma = 0.6$ S/m, $\varepsilon_r = 60$ and $\rho = 1000$ (kg/m^3) [15].

Figures 10 and 11 show, respectively, the induced current density and electric field calculated inside the human body due to HF radiation.

The maximum coupling conditions (uniform field along the body) are adopted in order to quantify in the most unfavourable conditions the maximum perturbation induced in the human body.

Figure 12 shows the induced values of SAR inside the body. The maximum values of the induced current density, the induced electric field and SAR at the feet are presented in Table 3.

The results presented in Figures 10 and 11 show that the induced electric field decreases gradually as one approaches to the axis of the equivalent cylinder. Namely, at high frequencies, the induced current moves to the periphery of the cylinder due to skin effect. The outer layers of the body behaves like a "shielding".

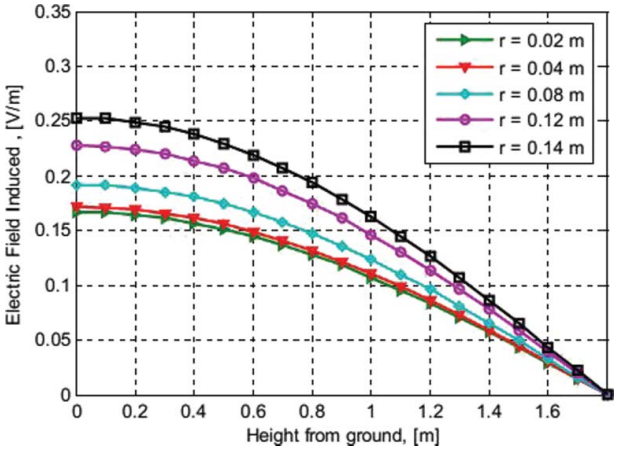

Figure 11. Calculated electric field inside the human body E_z = 1 V/m, f = 30 MHz.

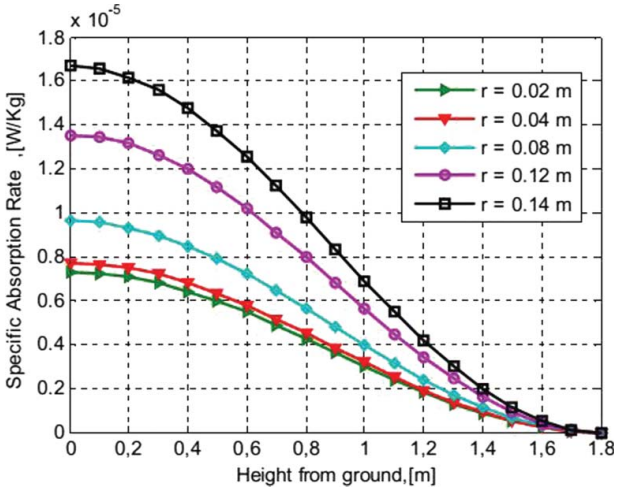

Figure 12. Calculated specific absorption rate (SAR) inside the human body $E_z = 1$ V/m, $f = 30$ MHz.

Table 3. Maximum values of the induced current density, electric filed and specific absorption rate in the feet.

	$J_z(a,0)$ (A/m^2)	$E_{(z=0)}$ (V/m)	$SAR_{(z=0)}$ (W/kg)
$f = 30$ MHz$a = 0.14$ m	0.1318	0.2534	1.6693×10^{-5}

The obtained results are compared to the exposure limits proposed by ICNIRP (SAR = 0.4 W/kg for General population, SAR = 0.08 W/kg for Occupational). The SAR values do not exceed the basic restrictions ($SAR_{max} = 1.6693 \times 10^{-5}$ W/Kg) and, as such, we conclude that heating effect is negligible.

Finally, the behaviour SAR versus frequency in the range from 5 to 40 MHz is analyzed.

The body model consists of a material with parameters simulating a muscle tissue: the frequency-dependent permittivity and electrical conductivity (see Table 4) [15].

The incident electric field amplitude is $E_z = 1$ V/m, and the maximum values of the SAR at the feet obtained for $J(r = a, 0)$ are shown in Table 5.

Table 4. Electrical parameters for a few frequencies.

Frequency (MHz)	Electrical conductivity, σ (S/m)	Relative permittivity, ε_r
5	0.54	150
15	0.56	100
20	0.57	80
30	0.6	60
35	0.66	53
40	0.7	50

Table 5. Maximum values of the SAR inside the human body.

Frequency (MHz)	SAR_{max} (W/Kg) for $J(r = a,0)$
5	6.0333×10^{-10}
15	9.0103×10^{-8}
20	4.3463×10^{-7}
30	1.6693×10^{-5}
35	2.4612×10^{-4}
40	2.4223×10^{-3}

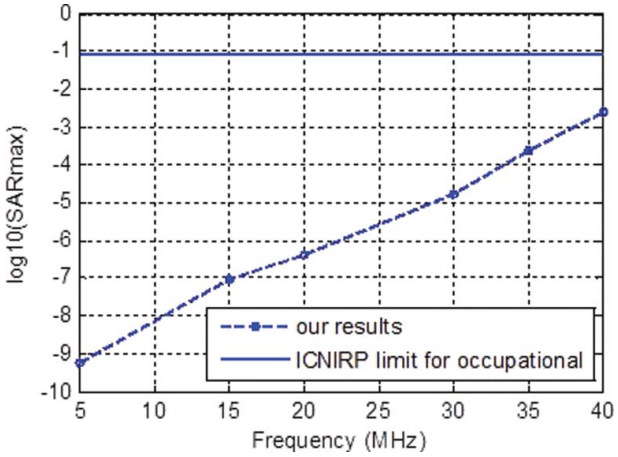

Figure 13. SAR_{max} values as a function of frequency.

According to Table 5, we remark that at range frequency 5–40 MHz, the SAR inside the human body increases rapidly with frequency. The main conclusion is that the SAR_{max} for different frequency never exceeds the limit of 0.08 W/kg defined by ICNIRP; moreover, the SAR depends on the frequency.

Figure 13 shows the logarithm of frequency-dependent SAR: log10(SAR_{max}).

The obtained results stay far below the ICNIRP exposure limits.

5. Conclusion

In this study, the transient-induced current and SAR induced in the human body when exposed to transient and time-harmonic radiation, respectively, are evaluated by using the enhanced TL theory. The simplified representation of the human body is related to the thick cylinder with the thin wires attached to account for the influence of the arms, thus extending the previous study of the authors dealing with the single-cylinder body model. The external electromagnetic field that excited the body is represented by equivalent current and voltage generators.

The proposed TL approach, compared to other more sophisticated numerical methods, provides fairly conclusive results for the transient-induced current and SAR for different cases of human exposure.

Therefore, this method (approach), considered reliable, represents a simplified tool for the assessment of the current induced in the human body due to both transient and time-harmonic electromagnetic field exposure, respectively, thus providing the rapid estimation of the phenomena and ensuring the useful results in an engineering sense.

Disclosure statement

No potential conflict of interest was reported by the authors.

References

[1] Dimbylow P. Development of the female voxel phantom, NAOMI, and its application to calculations of induced current densities and electric fields from applied low frequency magnetic and electric fields. Phys Med Biol. 2005;50(6):1047–1070.

[2] Hirata A, Yamazaki K, Hamada S, et al. Intercomparison of induced fields in Japanese male model for ELF magnetic field exposures: effect of different computational methods and codes. Radiat Prot Dosimetry. 2010;138(3):237–244.

[3] Poljak D, Tham CY, Kovac N. The assessment of human exposure to low frequency and high frequency electromagnetic fields using the boundary element analysis. Eng Anal Bound Elem. 2003;27:999–1007.

[4] Poljak D. Advanced modeling in computational electromagnetic compatibility. New York: Wiley; 2007.

[5] Mezoued S, Nekhoul B, Poljak D, et al. Human exposure to transient electromagnetic fields using simplified body models. Eng Anal Bound Elem J. 2010;34(1):23–29.

[6] Paul CR. Analysis of multiconductor transmission lines. New York (NY): Wiley Interscience; 1994. p. 641–692.

[7] Ametani A, Kasai Y, Sawada J, et al. Frequency dependent impedance of vertical conductors and a multiconductor tower model. IEE Proc-Gener Trans Distrib. 1994;141(4):339–345.

[8] Rojers EJ, White JF. Mutual coupling between finite lengths of parallel or angled horizontal earth return conductors. IEEE Trans Power Deliv. 2005;4(1):103–113.

[9] Taylor CD, Satterwhite RS, Harrison CW Jr. The response of terminated two-wire transmission line excited by a non uniform electromagnetic field. IEEE Trans Antenn Propag. 1965;AP-13:987–989.

[10] Paul CR. A spice model for multiconductor transmission lines excited by an incident electromagnetic field. IEEE Trans Electromagnet Compat. 1994;36(4):342–354.

[11] Poljak D. Average power and total energy absorbed in the human body exposed to transient fields. Proceedings of the 12th IEEE Mediterranean Electrotechnical Conference (MELECON); 2004 May 12–15; Dubrovnik, Croatia, vol. 2. 2004. p. 507–510.

[12] Kaune WT, Forsythe WC. Current densities measured in human models exposed to 60-Hz electric fields. Bioelectromagnetics. 1985;6(1):13–32.

[13] Poljak D, Tham CY, Gandhi O, et al. Human equivalent antenna model for transient electromagnetic radiation exposure. IEEE Trans Electromagnet Compat. 2003;45(1):141–145.

[14] ICNIRP Guidelines. Guidelines for limiting exposure to time-varying electric, magnetic, and electromagnetic fields (up to 300 GHz). Health Phys. 1998;74:494–522.

[15] Gabriel S, Lau RW, Gabriel C. The dielectric properties of biological tissues: II. Measurements of the frequency range 10 Hz to 20 GHz. Phys Med Biol. 1996;41(11):2251–2269.